Investigation of electrodeposition of Ni–Co–Fe–Zn alloys in DMSO with MHD effect

Mehdi Ebadi[a,b,], Wan Jeffrey Basirun[a], Yatimah Alias[a],*
Mohammad Reza Mahmoudian[a,c], Sim Yoke Leng[a,d]

[a]*Department of Chemistry, Faculty of Science, University of Malaya, 50603 Kuala Lumpur, Malaysia*
[b]*Department of Chemistry, Gorgan Branch, Islamic Azad University, Gorgan, Iran*
[c]*Department of Chemistry, Masjed-Soleiman Branch, Islamic Azad University, Masjed-Soleiman, Iran*
[d]*Department of Chemical Science, Faculty of Science, University Tunku Abdul Rahman, Jalan Universiti, Bandar Barat, 31900 Kampar, Perak, Malaysia*

ARTICLE DATA

ABSTRACT

This paper reports the magneto-electrodeposition of the Ni–Co–Fe–Zn alloys by chronoamperometry in Dimethyl Sulfoxide solvent in the presence and absence of a Permanent Parallel Magnetic Field (PPMF) to the cathode surface. It was found that the deposition current in the presence of PPMF (9 T) was enhanced compared to the absence of PPMF. The current enhancement percentage ($\eta\%$) was increased when deposited in the presence of PPMF ($\eta\% = 2\pm0.07\%$, $15.78\pm0.93\%$ and $21.6\pm1.04\%$) for 1 h at -1.10, -1.20 and -1.30 V respectively. Deposition at higher potentials in the presence of PPMF was also found to increase the deposition efficiency. The Composition Reference Line for Ni was calculated to be around 25%, although the noble metals (i.e., Ni, Co) showed anomalous deposition behavior in the presence of the less noble elements like Zn and Fe. The nucleation and growth were also investigated during the electrodeposition process. It was shown that nucleation and diffusion coefficients were promoted when using PPMF and increasing of applied potential. The corrosion behavior of the alloy surface was examined by the Open Circuit Potential and Electrochemical Impedance Spectroscopy. The results showed that the corrosion resistance increased with the increase of content of more noble metals.

1. Introduction

Alloy electrodeposition, is a surface finishing technique which has been used to improve properties such as grain size, hardness, and corrosion resistance compared to the parent metals. The main problem of metal electrodeposition process in an aqueous bath is the Hydrogen Evolution Reaction (HER) which affects the morphology of the electrodeposited surface. To avoid the HER, metal and alloy electrodeposition in organic solvents was investigated by several researchers [1–4], and also as a method to improve the surface of the electrodeposited layers. Dimethyl Sulfoxide (DMSO) is one of the organic aprotic solvents which has been used in electrodeposition of metals [5–7].

An example of alloy electrodeposition used in surface improvement is the electrodeposition of Zn with iron group elements (i.e. Fe, Ni, Co). The main problem in alloy electrodeposition of these metals is their anomalous behavior.

* *Corresponding author at:* Department of Chemistry, Faculty of Science, University of Malaya, 50603 Kuala Lumpur, Malaysia. Tel.: +60 172097738; fax: +60 3 79674193.
  E-mail address: mehdi_2222002@yahoo.com (M. Ebadi).

Researchers have faced this problem since 1907. Alloy electrodeposition of the Zn–Iron group elements exhibited the problem of anomalous deposition where the less noble metals (i.e. Zn) deposits preferentially compared to the more noble metals (i.e., Ni>Co>Fe). Several theories have been developed [2–4] to describe this anomalous behavior. Dahms and Caroll [8] explained that the anomalous phenomenon is related to the Hydroxide Suppression Mechanism (HSM). This theory suggested that the more noble ions were hindered from electrodeposition by the formation of the less noble ion hydroxides. This theory is further supported by the solubility constant (K_{sp}) of $M(OH)_n$ where the K_{sp} of Zn<Fe<Co<Ni.

Several investigators [9–12] have studied the effects of pH, current density (potential range), temperature and the counter anions on the anomalous deposition. Some investigators [9,13] found that the pH in the vicinity of the cathode was increased during alloy electrodeposition, but others [8,9] disagreed with those statements. Electrodeposition of the noble metal ions increases with the increase pH of the electrolyte [13,15]. The anomalous phenomenon decreases the tendency towards natural deposition with the increase of temperature [9]. Apart from the HSM theory, some authors [11–18] found that Under Potential Deposition (UPD) of the less noble ions also led to anomalous electrodeposition. Normal co-deposition takes place at lower potentials whereas anomalous co-deposition occurs when the potential range increases [19,20]. The type of anions also affects the UPD behavior, i.e., with increasing I^- concentration in the zinc electrolyte, the peak of the Zn electrodeposition shifts to more negative potentials whereas with increasing PO_4^{3-} concentration, the peak shifted to more positive potentials [12] in the voltammograms.

Electrodeposition in the presence of magnetic field is a well established phenomenon. The application of a magnetic field parallel to the cathode surface increases the mass transport of ions to the surface and this phenomenon is known as the Magneto-Hydrodynamic (MHD) effect. This effect accounts for five types of forces which act on the ions and increases the mass transport. The most dominant forces are the Paramagnetic force ($\vec{F}_P$) and Lorentz force ($\vec{F}_L$) which increase the convection of charged species and influences the deposit morphology. The Lorentz force ($\vec{F}_L$) plays a major role in the convection of charged species and is the largest among the five forces. However, the Paramagnetic force ($\vec{F}_P$) acts on the paramagnetic ions only. The Lorentz force is due to the interaction between magnetic flux (B) and electrical current and is described by:

$$\vec{F}_L = (B \times j) \qquad (1)$$

where j is the current density. The Lorentz force is maximal if the magnetic field is exerted perpendicular to the direction of the cathodic current. This paper describes the effect of a Permanent Parallel Magnetic Field on the mass deposition of Ni–Co–Fe–Zn alloy layers in DMSO solvent. Up to date, the electrodeposition of these alloys in the presence of a magnetic field in organic solvents has not been reported. Furthermore, it was found that the major element of the electrodeposited Ni–Co–Fe–Zn alloy from aqueous solution was zinc, which means that the anomalous phenomenon was present with less noble ions (in this case, Zn) [21], where zinc is a diamagnetic element.

2. Experimental

Copper plates were used as working electrodes. One side (0.1×1×1 cm) of each plate was electrochemically polished and activated by immersion into mixed acids (HCl 30%–H_2SO_4 10%–HNO_3 5%–CrO_3 3%) for a few seconds and then rinsed with double distilled water and dried in oven. The stock solution for the Ni–Co–Fe–Zn alloy electrodeposition contained 1 M $NiCl_2.6H_2O$, 0.25 M $CoCl_2.6H_2O$, 0.25 M $FeCl_2.4$-H_2O and 0.25 M $ZnCl_2$ dissolved in DMSO. The electrolyte was free from additives such as levelers and brighteners. The electrolyte was kept at room temperature and at neutral pH. The experiments were carried out using chronoamperometry method at potentials of −1.10, −1.20 and −1.30 V with a three-electrode set up using a Princeton Applied Research (PAR) Versa STAT3 instrument. Electrodeposition was performed both in the absence and presence of PPMF (9 T). In addition, eight types of electrolyte (Ni, Co, Fe, Zn, Ni–Co, Ni–Co–Fe, Ni–Co–Zn and Ni–Co–Fe–Zn) were prepared where the concentration of each element was adjusted to 0.01 M for each electrolyte. Voltammetry and chronoamperometry in the presence and absence of PPMF (9 T) were done in a Teflon cell at room temperature.

Saturated Calomel Electrode (SCE) and platinum wire were used as the reference and counter electrodes respectively. The corrosion behavior of the alloy surface was tested with the Open Circuit Potential (OCP) and Electrochemical Impedance Spectroscopy (EIS) in 3.5% NaCl solution. EIS was done on the Ni–Co–Fe–Zn alloys with V_{rms} of 5 mV around the OCP with a frequency range of 10 kHz to 10 mHz. The topography of the deposited layers was investigated via Atomic Force Microscopy (AFM PS 3000-NS3a). The alloy electrodeposits were analyzed using X-ray Diffraction (D_8-Advanced XRD) with Cu K_α radiation of wavelength 1.540 Å. The mass of electrodeposition was calculated from the weight difference of the bare and coated Cu substrates. Scanning Electron Microscopy (SEM-FEI Quanta 200F) was used to capture images of the surface morphology of the alloy samples. Elemental composition was done using Energy Dispersive X-Ray analysis with the Energy Dispersive System INCA energy 400.

3. Results and Discussion

3.1. Cyclic Voltammetry and Chronoamperometry

Fig. 1 shows the voltammograms of Ni, Co, Fe, Zn, Ni–Co, Ni–Co–Fe, Ni–Co–Zn and Ni–Co–Fe–Zn electro-reduction in DMSO with the presence and absence of PPMF (9 T). Fig. 1A–D shows that the onset potential of electro-reduction of metal ions became more negative in the order of Ni>Co>Fe>Zn. The influence of the PPMF towards the increase of the electrodeposition current can be seen in these results. These results are in accordance with the Navier–Stokes equation (Eq. (2)) [22,23]:

$$j_l = \left(4.3 \times 10^3\right) n^{3/2} A^{3/4} D.v^{-1/4} C^{4/3} B^{1/3} \qquad (2)$$

where j_l is the current (A cm^{-2}), v is the viscosity of solution (cm^2 s^{-1}), C is the bulk concentration of electroactive species
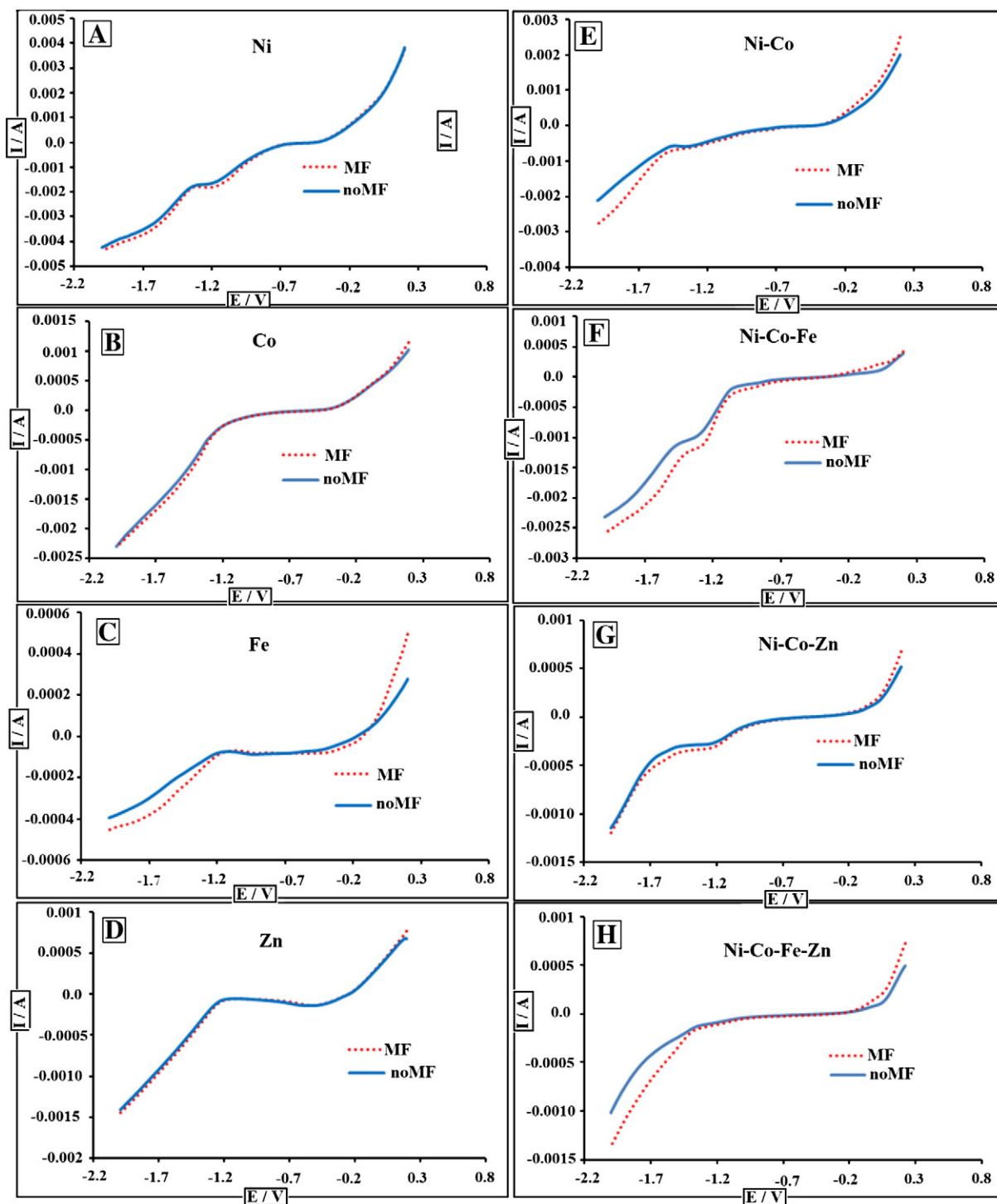
Fig. 1 – Cyclic voltammogram of: A) Ni, B) Co, C) Fe, D) Zn, E) Ni–Co, F)Ni–Co–Fe, G) Ni–Co–Zn, H) Ni–Co–Fe–Zn in DMSO, in the presence and absence of PPMF (9 T). Concentration of each solution was set at 0.01 M during CV.

(mol cm^{-3}), B is the strength of a magnetic field (T), D is the diffusion constant (cm^2 s^{-1}), A is the electrode surface area (cm^2), n is the number of electrons involved in the electron transfer step and the numerical constant has units of cm mol$^{-1/3}$ T$^{-1/3}$ s$^{-1/4}$.

Fig. 1H affirms the theory of UPD where the electrodeposition potential shifts to positive direction for the Ni–Co–Fe–Zn alloy compared to the electrodeposition of the pure metals (i.e.

Zn, Fe). Fig. 1H shows that the onset potential for the electro-reduction of Ni–Co–Fe–Zn alloy is more positive (around −1.0 V) than the onset potential of electro-reduction in Fig. 1C and D for Fe (−1.20 V) and Zn (−1.22 V) respectively. In accordance with Eq. (2), Fig. 1 shows that the current increases in the presence of PPMF compared to the absence of PPMF. It must be noted that these results are obtained in DMSO solvent

which has larger viscosity compared to water (1.987 mPa s^{-1} and 0.890 mPa s^{-1} respectively at 25 °C). Our previous results in aqueous solution [21] gave larger increase of electro-reduction currents in the presence of PPMF compared to the absence of PPMF. But the increase of the reduction currents with PPMF compared to without PPMF in DMSO solvent is lower, and this is also in accordance with Eq. (2).

The electrodeposition of the Ni–Co–Fe–Zn alloys is performed using chronoamperometry at various potentials (−1.10 V, −1.20 V and −1.30 V) with and without the presence of the PPMF (9 T). Fig. 2 shows the chronoamperometry results where the current |I$_i$| increases with the presence of PPMF. The current increase is due to the Magneto-Hydrodynamic (MHD) effect, which is largely due to the effect of the Lorentz force in the presence of the magnetic field. The electrodeposition mass also increases in the presence of PPMF. Fig. 2 also shows that the difference in the current value (ΔI) with and without PPMF (9 T), increases significantly with the increase of the applied potential, i.e., ΔI for −1.30 V > ΔI for −1.20 V > ΔI for −1.10 V. It could be deduced that the Lorentz force also increases with the increase of the current density due to the greater interaction between magnetic flux and electrical current (Eq. (1)). The increases of deposition current |I$_i$| in the absence compared to the presence of the PPMF are: 5.00×10^{-4} to 5.10×10^{-4} mA cm^{-2}, 1.52×10^{-3} to 1.76×10^{-3} mA cm^{-2}, 2.68×10^{-3} to 3.26×10^{-3} mA cm^{-2} at potentials of −1.10, −1.20 and −1.30 V respectively, as shown by marked points (¤) in Fig. 2. The current enhancement percentage calculated at the marked points by the following equation [24]:

$$Current\ enhancement\ \Gamma\% = \frac{\Delta I}{I_i} \times 100 \tag{3}$$

where ΔI is the difference of the current in the presence and absence of PPMF (9 T) and I$_i$ is the current in the absence of PPMF. The current enhancement percentages (η%) were calculated as η% = 2±0.07%, 15.8±0.93% and 21.6±1.04% for depositions at −1.10, −1.20 and −1.30 V respectively, for 1 h deposition time.

According to Fig. 3, the absolute value of I–t transient has a normal dependency with the applied potential. It was shown that the nucleation and growth process for electrodeposition of Ni–Co–Fe–Zn alloys is not entirely diffusion-controlled which will be described later. The surface coverage (θ) for
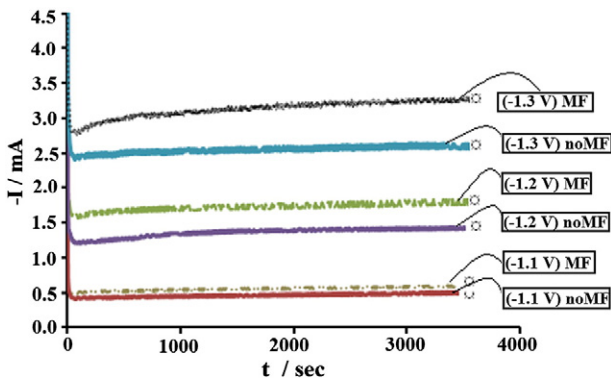

Fig. 2 – Chronoamperometry of Ni–Co–Fe–Zn alloy electrodeposition in the presence and absence of PPMF (9 T) at applied potentials of −1.10, −1.20 and −1.30 V.
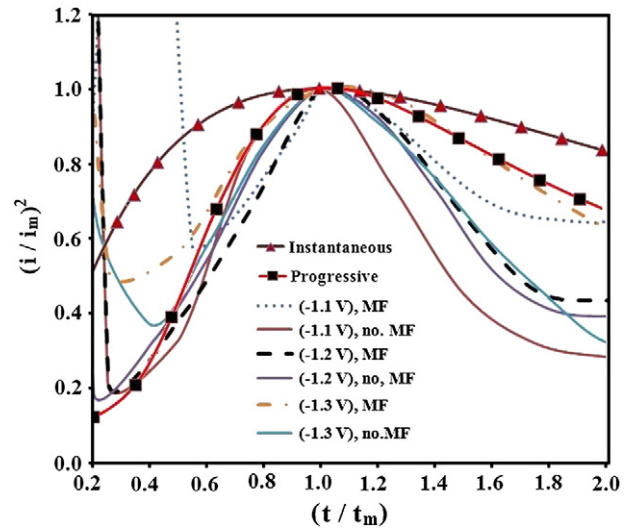

Fig. 3 – The (i/i$_m$)^2 vs t/t$_m$ curves for deposition of the Ni–Co–Fe–Zn alloys from DMSO solution in the absence and presence of PPMF and different amounts of applied potential which are compared to instantaneous and progressive calculate curves.

nucleation can be increased by increasing the current density [20]. For long time process, the current transient is given by:

$$I_t = \frac{nAFD^{1/2}\sum C^\infty}{\pi^{1/2}t^{1/2}} \tag{4}$$

where A is area of electrode (cm^2), D is the diffusion coefficient (cm s^{-1}), C$^\infty$ is the bulk concentration of ions (mol cm^{-3}), t is the time of electrodeposition process and n is the number of electrons.

The non-dimensional relation of i^2/i^2_m vs. t/t$_m$ was plotted from the maximum i$_m$ and t$_m$ in the i–t transients during the electrodeposition process. Nucleation and growth propagation during electrodeposition can be described from the I–t transients in Fig. 3. However, the rate of growth is a function of electroactive species, current density, double layer, and viscosity of bulk electrolyte. The nucleation process was described by Scharifker and Hills [20] from the theory of non-dimensional transients i.e., instantaneous (Eq. (5)) and progressive (Eq. (6)). The slow growth of nucleation on small number of activation sites during the initial time of the process could be described by instantaneous nucleation mechanism. However progressive nucleation takes place when the rate of new nuclei formation continues over longer periods of time and the fast growth of nuclei occurs on many active sites. Fig. 3 shows the typical plots together with theoretical curves from a modified Scharifker equation [25] for the instantaneous and progressive nucleation for the Ni–Co–Fe–Zn alloy at different applied potentials. The chronoamperometric curves (Fig. 3) for the instantaneous and progressive nucleation are given in Eqs. (5) and (6) respectively.

$$\left(\frac{i(t)}{i_{max}}\right)^2 = \frac{1.9542}{t/t_{max}}\left\{1 - \exp\left[-1.2564\left(\frac{t}{t_{max}}\right)\right]\right\}^2 \tag{5}$$

$$\left(\frac{i(t)}{i_{max}}\right)^2 = \frac{1.2254}{t/t_{max}}\left\{1-\exp\left[-2.3367\left(\frac{t}{t_{max}}\right)^2\right]\right\}^2 \tag{6}$$

where the i_{max} and t_{max} correspond to the maximum peak current in the chronoamperometric diagrams and the time taken to reach the peak current, respectively. The diagrams (Fig. 3) show that the electrodeposition of Ni–Co–Fe–Zn alloy is closer towards progressive nucleation taking into account the eventual overlap of diffusion zones [25]. According to Gunawardena et al. [20], the relationship of i vs. t, at a very short time frame ($N_0t{\rightarrow}0$), progressive nucleation (AN_0) can be defined by the following equation:

$$i(t) = \frac{2zFAN_0\pi(2DC)^{3/2}M^{1/2}t^{3/2}}{3\rho^{1/2}} \tag{7}$$

where C is the bulk concentration of species, D is the diffusion coefficient determined from the deposition transient, zF is the molar charge of electrodepositing species, A is the nucleation rate constant, i_{max} is the current maximum at critical time (t_{max}), ρ is the density of the electrodeposited layer for alloys which is function of alloy equivalent weight (M):

$$M = \frac{1}{\sum \frac{n_i f_i}{A_i}} \tag{8}$$

In Eq. (8), n_i is the valence of the alloy element 'i', f_i is the mass fraction of the alloy element 'i' and A_i is the atomic mass of element 'i'. The diffusion coefficient can be calculated when the current maximum occurs at a time:

$$t_m = \left(\frac{4.6733}{AN_0\pi K^{'}D}\right)^{1/2} \tag{9}$$

With a maximum current density;

$$i_m = 0.4615zFD^{3/4}C\left(AN_0K^{'}\right)^{1/4} \tag{10}$$

where $K^{'} = \frac{4}{3}\left(\frac{8\pi CM}{\rho}\right)^2$, and the product of $i_m^2 t_m$ yields:

$$i_m^2 t_m = 0.2598(zFC)^2 D \tag{11}$$

The diffusion coefficient can be determined from the product of ($i_m^2 t_m$) which is independent of the nucleation and growth rate [20]. Table 1 shows that the number of nucleation

Table 1 – Compression of the current and time maxima affected by cysteine concentration, and the calculated nuclear number, diffusion coefficient and height of depositing layers.

App. potential: E (V)	I_{max} (mA cm^{-2})	t_{max}(s)	AN_0 ($\times 10^{-6}$ cm^{-2})	$D\times 10^6$ (cm^2 s^{-1})
(−1.1 V), MF	−0.6347	11	0.9273	0.157
(−1.1 V), no MF	−0.9756	4	0.4141	0.112
(−1.2 V), MF	−2.8782	4	1.0385	1.126
(−1.2 V), no MF	−2.1682	5	0.9688	0.793
(−1.3 V), MF	−5.5515	4	1.686	4.161
(−1.3 V), no MF	−4.0700	5	1.6731	2.792

sites and diffusion coefficient is increased due to the increase of applied potential (from −1.1 to −1.3 V) and the presence of PPMF. The calculated diffusion coefficient increases with the presence of PPMF and tabulated in Table 1. The falling portion of i–t transient (Fig. 3) could be analyzed to study the initial transient stages.

3.2. Mass Electrodeposition

Fig. 4 shows the massograph of the electrodeposited Ni–Co–Fe–Zn alloy calculated from the difference of the bare and coated Cu plates. The mass electrodeposition increases with the increase of potential from −1.10 to −1.30 V. This phenomenon could be explained by the increase in the current due to the decrease of diffusion layer caused by the MHD effect in the presence of PPMF. As aforementioned, the difference between mass deposition of alloys with and without PPMF increases with the increase of applied potential. The mass of electrodeposition increases in the presence of PPMF [20]. Aboubi et al. [26] have also shown that the current (i_l) is inversely proportional to the viscosity of solution v, but proportional to the bulk concentration of electroactive species C, the electrode surface area A, the magnetic flux B, the diffusion coefficient D, and the number of electrons n, as given in Eq. (2).

The relationship between the magnetic flux and mass increase can be given by the Navier–Stokes equation [27] and [28]:

$$m \approx 0.63(\rho R)^{-1/3}.v^{-2/9}.D^{8/9}.(nFcB)^{1/3} \tag{12}$$

where R is the electrode radius, F is the Faraday constant, ρ the density of solution and other parameters as mentioned previously.

Fig. 4 gives the mass electrodeposition rate with various current densities in the presence and absence of PPMF, which could also be supported by Eq. (12). Our previous results [20,21,29–31] have shown that the mass of electrodeposition with PPMF is greater than the mass of electrodeposition without PPMF. Furthermore, the difference between the mass of electrodeposition with the presence and the absence of the PPMF increases with the increase of the current density. Noteworthy, the electrodeposition efficiency of Ni–Co–Fe–Zn alloys increases due to the presence of PPMF (9 T) compared to the
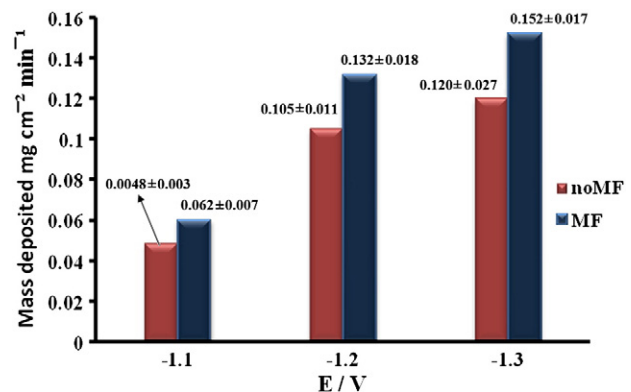
Fig. 4 – Mass electrodeposition rate of Ni–Co–Fe–Zn alloys in the presence and absence of PPMF.

absence of PPMF, from 63.22% to 66.11% (at −1.1 V), from 65.27% to 72.27% (at −1.2 V), and from 69.96% to 80.10% (at −1.3 V). Significantly, it was also found that the increase in deposition potential led to the increase in deposition efficiency.

Notably, the limitations of alloy electrodeposition in higher viscosity DMSO solvent compared to aqueous solutions are slower ion transport and lower ionic conductivity. Furthermore, the presence of carbon was found in the EDX results (inset of Fig. 5) at higher applied potential. The detected carbon on the deposits could be due to the decomposition of DMSO solvent.

3.3.   SEM/EDX

Scanning Electron Microscopy (SEM) was used to investigate the surface morphology of the electrodeposited Ni–Co–Fe–Zn alloy. The SEM images (Fig. 5A, C) and (Fig. 5B, D) are alloy surfaces deposited at −1.10 V and −1.30 V respectively. Fig. 5C and D images are alloy surface which are deposited in the presence of PPMF (9 T). Several researchers [26] and [32] reported that the magnetic field affects the deposit morphology. Micro-cracks appear on the surface layers (Fig. 5B and D) which are deposited at more negative potentials −1.30 V, and these cracked surface images are also similar to that reported for the deposition of platinum on copper substrate [33] and [34]. But Fig. 5D shows fewer micro-cracks compared to

Fig. 5B with the same deposited potential. Zielinski et al. [35] have found that the stress on the surface could be reduced by using magnetic field during the electrodeposition process, which could lead to fewer micro-cracks on the surface. They have also reported that the micro-cracks appeared due to heat and free entropy of adsorption of charged species. The EDX spectrum taken together with the SEM shows that the alloy surface contained only Ni, Co, Fe and Zn. From the EDX results (Fig. 6), it was found that the Ni content on the electrodeposited alloy surface was always lower than the Composition Reference Line (CRL) due to the anomalous behavior. In this case, the CRL of Ni is defined as [19]:

$$CRL = \frac{c\left(Ni^{+2}\right)}{\left[c\left(Ni^{+2} + Co^{+2} + Fe^{+2} + Zn^{+2}\right)\right]} \times 100 \qquad (13)$$

where c is the concentration of each ion (i.e., c (Ni) is the concentration of Ni^{2+} in electrolyte). From the EDX results, it can be seen that the weight percentage (wt.%) of Fe became smaller with the increase of current density due to the increase of applied potential. The anomalous behavior could be seen from the CRL in Fig. 6. The CRL for Ni (25%) was calculated and marked in Fig. 6. Notably, the lowest deposition content belonged to Zn. The co-electrodeposition of Zn with Fe, Co, and Ni did not occur at deposition potential of −1.10 V, but
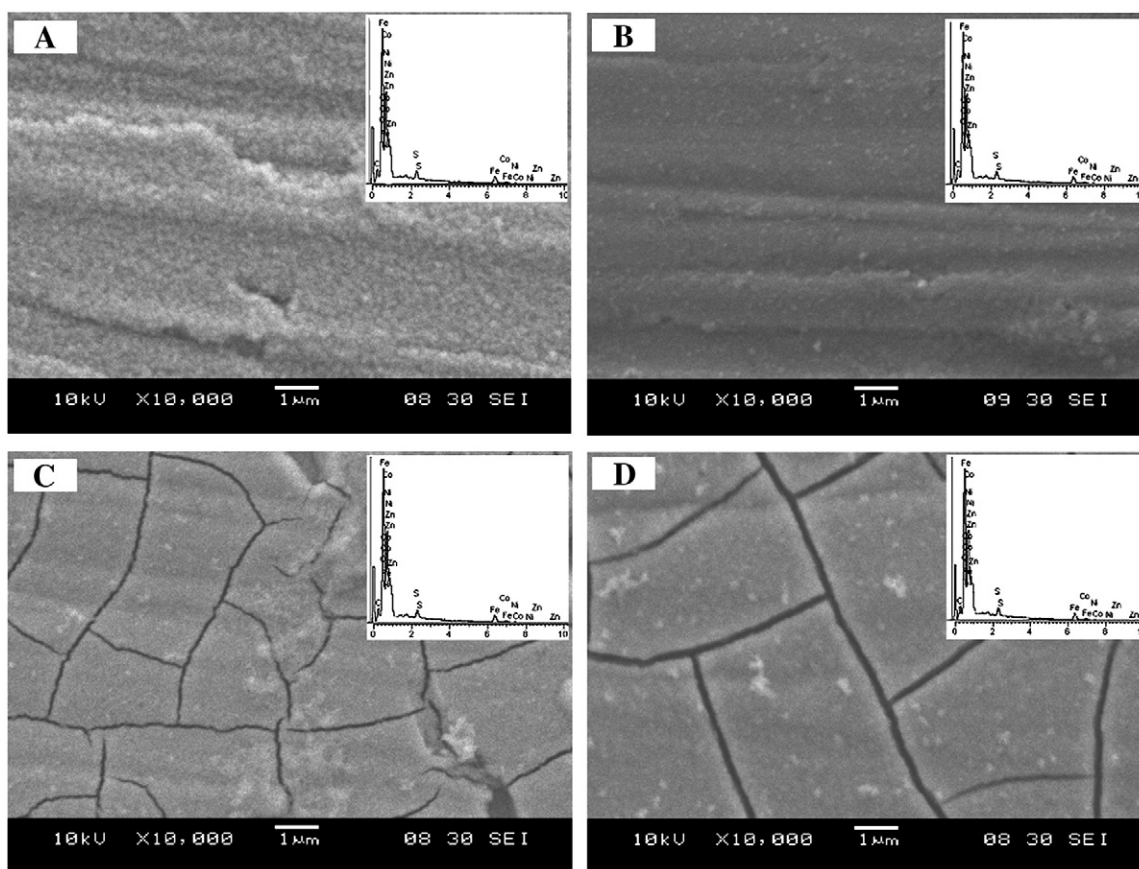

Fig. 5 – The SEM micrographs (magnification 10000×) of Ni–Co–Fe–Zn electrodeposited without PPMF: A) −1.10 V, B)−1.30 V, and with PPMF (9 T), C) −1.10 V, D) −1.30 V. The SEM images were marked with EDX to show the composition of electrodeposited layers.
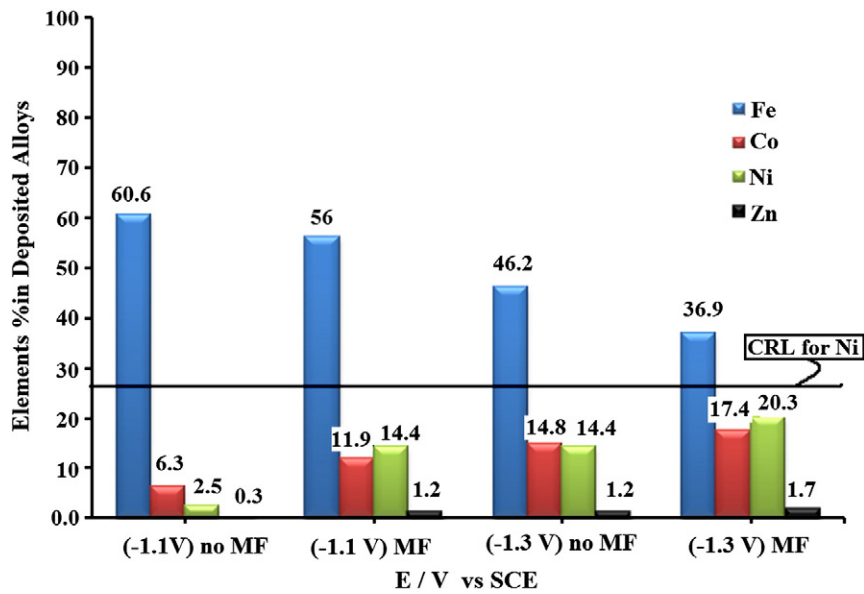
Fig. 6 – EDX results of the percentage of metal elements with the deposition potential.

the Zn content became higher with the increase of deposition potential. For electrodeposition of the Ni–Co–Fe–Zn alloys at −1.10 and −1.30 V, the anomalous behavior was mainly shown by Fe^{2+} due to the UPD in DMSO. Noteworthy that the oxidation of Fe^{2+} to Fe^{3+} was not observed in DMSO due to the low amount of oxidation agents (e. g., H_2O). This result is quite different from our previous results where the anomalous deposition was shown by Zn^{2+} from electrodeposition
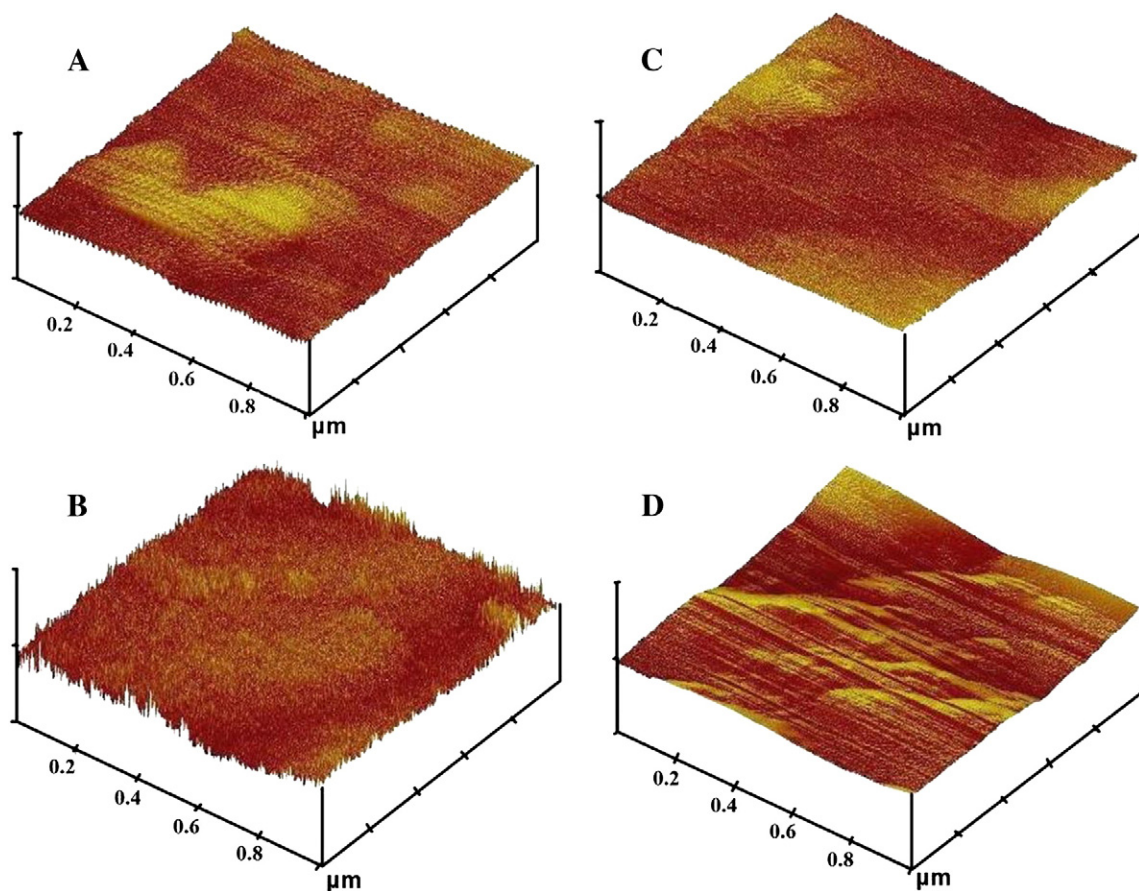

Fig. 7 – AFM images of Ni–Co–Fe–Zn alloy surface electrodeposited in the absence of PPMF: A) −1.10 V, B) −1.30 V, and with PPMF (9 T): C) −1.10 V, D) −1.30 V.

in aqueous solution [21]. The anomalous behavior in the electrodeposition of Ni–Co–Fe–Zn alloys is diminished when using PPMF and at higher applied potential of −1.30 V [19].

3.4. AFM Studies

Atomic Force Microscopy (AFM) was used to determine the surface roughness of the Ni–Co–Fe–Zn alloys. Fig. 7 shows the 3D AFM images of the Ni–Co–Fe–Zn alloy surface deposited with and without the presence of PPMF (9 T). The 3D AFM images were prepared at the same vertical scale from a scanning surface of 1×1 μm. The surface images in Fig. 7A and C were obtained at −1.10 V deposition potential whereas the surface images in Fig. 7B and D were obtained at −1. 30 V deposition potential. The 3D AFM images of the alloys electrodeposited in the presence of PPMF are on the right (Fig. 7A and B), while the 3D images of the alloys electrodeposited in the absence of the PPMF are on the left (Fig. 7C and D). These results show that the surface became smoother when electrodeposited using PPMF under the same conditions. The smoother electrodeposited surface could be due to the decrease of the double layer when the PPMF was present. At the applied potential of −1.10 V, the roughness factor was reduced from 10.55 nm (without PPMF) to 9.06 nm (with PPMF). Furthermore, at the applied potential of −1.30 V the roughness factor was reduced from 16.67 nm (without PPMF) to 9.22 nm (with PPMF). These results are in accordance with our previous results [20]. Fahidy [36] has also investigated the influence of PPMF on the dendrites and branches on the electrodeposited surface although the effect of the magnetic field towards a more even electrodeposited surface is still unclear.

3.5. OCP and EIS

The corrosion behavior of the Ni–Co–Fe–Zn electrodeposited alloys from DMSO was studied. Two types of electrochemical measurements were used to determine the corrosion resistant properties of the Ni–Co–Fe–Zn alloy surface, which are the Open Circuit Potential (OCP) and Electrochemical Impedance Spectroscopy (EIS). Four samples with different elemental compositions were tested in these experiments. It was found that
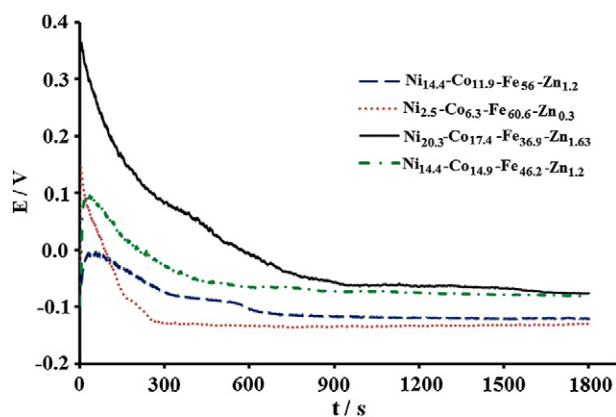
the surface with higher content of noble metals (i.e., Ni, Co) has more positive OCP. In these experiments, Fe is the sacrificial element. At longer measurement times, the curves became depressed to lower potentials, because of the oxidation of metallic Fe to Fe^{2+} and Fe^{2+} to Fe^{3+}. After the passivation of the surface of the plated layers has taken place, the steady state condition is achieved for longer measurement times as shown in Fig. 8.

EIS was done immediately after the OCP results were obtained. EIS was done on the alloy surface to analyze the "NaCl solution/Ni–Co–Fe–Zn alloys/Copper substrate" system. The parameters in the EIS (R, C and Q) were obtained using a simulation program which were compared with the results from experiments, where the equivalent circuit of R(Q [R(RC)])(RQ) was found to accurately fit the experimental results.

F. Mansfeld [37] and J.R. Scully [38] reported that most impedance data for coated metals which have been exposed to corrosive solution can be represented by the first part in the equivalent circuit diagram in Fig. 9.

The physical model of the "NaCl solution/Ni–Co–Fe–Zn alloy/Copper substrate" system which is represented by the equivalent circuit could be explained as follows. The R represents the NaCl solution resistance between the alloy surface and the RE, which can be written as R_s, where R_s was connected in series with a parallel circuit which consists of Q and R. The Q is the capacitance of the alloy coating, resulting from the pores in the Ni–Co–Fe–Zn alloy, from the corrosion in the sea water solution.

Instead of a pure capacitor, a Constant Phase Element (CPE) was introduced in the fitting procedure to obtain good agreement between the simulated and experimental data. The impedance of CPE is defined as $Z_{CPE} = Q^{-1} (j\omega)^{-n}$; where Q ($\Omega^{-1} s^n cm^{-2}$) is the combination of properties related to both the surface and the electroactive species, independent of frequency. The Q will be closer to capacitance if the n value becomes closer to 1, but it should be stressed that for simplicity Q is often considered as capacitance. The R is the pore resistance which can be written as R_P which represents the resistance towards ion conduction in the pores of the alloy layer.

The pore resistance R_p was connected in series with the second parallel combination of R and C, where R is the resistance towards the charge transfer which occurs across the "NaCl electrolyte/Ni–Co–Fe–Zn alloy" where corrosion
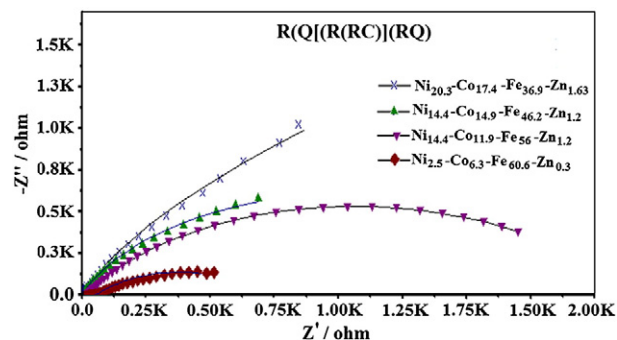
Fig. 8 – OCP measurements with time for deposited Ni–Co–Fe–Zn alloys with different compositions immersed in 3% NaCl solution for 1800 s.

Fig. 9 – Nyquist plots for Ni–Co–Fe–Zn alloy surface immersed in 3% NaCl solution at 1800 s immersion time. ×); $Ni_{20.2}$–$Co_{17.14}$–$Fe_{36.9}$–$Zn_{1.6}$ ▲); $Ni_{14.4}$–$Co_{14.8}$–$Fe_{46.2}$–$Zn_{1.2}$ ▼); $Ni_{14.4}$–$Co_{11.9}$–Fe_{56}–$Zn_{1.2}$ ♦); $Ni_{2.5}$–Co_{32}–$Fe_{60.6}$–$Zn_{0.3}$.

Table 2 – Simulated data from EIS for Ni—Zn alloys electrodeposited from DMSO solution.

Electrodeposited at:	Composition of layers	R_{ct} (kOhm)	C1 (μF)	Q1Y0 ($\Omega^{-1}(s)^n cm^{-2}$)	n
−1.3 V(PPMF)	$Ni_{20.3}-Co_{17.4}-Fe_{36.9}-Zn_{1.6}$	20.42	1.962	0.136e−02	0.779
−1.3 V	$Ni_{4.4}-Co_{14.8}-Fe_{46.2}-Zn_{1.2}$	10.39	2.532	0.349e−02	0.709
−1.1 V (PPMF)	$Ni_{4.4}-Co_{11.9}-Fe_{56}-Zn_{1.2}$	9.67	13.8	0.188e−02	0.666
−1.1 V	$Ni_{2.5}-Co_{32}-Fe_{60.6}-Zn_{0.3}$	7.59	28.05	0.566e−02	0.656

happens in the Ni–Co–Fe–Zn pores and can be written as R_{ct}. Therefore the R_{ct} is the measure of the corrosion resistant property of the alloy in the pores surface. The parallel combination with the R_{ct} is the double layer capacitance C, which can be written as C_{dl} and this is the double layer capacitance across the "NaCl electrolyte/Ni–Co–Fe–Zn alloy" in the pores.

The third parallel combination of R and C is for the copper substrate, where the corrosion has reached the copper substrate. The R is the charge transfer resistance for the corrosion reaction which occurs across the "NaCl electrolyte/Cu substrate" and can be written as R_{ctc}. Q is the CPE for the corrosion reaction which occurs across the "NaCl electrolyte/Cu substrate" which can be written as Q_c. The overall equivalent circuit diagram which represents the "NaCl solution/Ni–Co–Fe–Zn alloys/Copper substrate" system can be written as $R_s(Q[R_p(R_{ct} C_{dl})])(R_{ctc} Q_c)$.

Fig. 9 also showed that the diameter of semi-circles decreased in the presence of the less noble metal (i.e., Fe). Table 2 gave the values of R_{ct} obtained from the curve fitting procedure, which shows that R_{ct} values decrease in the presence of the less noble metals, in this case Fe. It also illustrates that the corrosion resistance of the alloys increase with the increase of deposition potential and with the presence of the PPMF. The electrodeposited alloys show stronger resistance against corrosion in the presence of more noble metal Ni and Co.

4. Conclusion

The influence of the magnetic field (9 T) aligned parallel to the cathode surface, on the electrodeposition of Ni–Co–Fe–Zn alloys in DMSO solution was studied at room temperature. The PPMF influence on the electrodeposition reaction is by decreasing the double layer thickness and thus increasing the current density and the mass deposition. The increase of deposition current is shown in the voltammogram in the presence of PPMF (9 T). From chronoamperometry, the increase in electrodeposition potential causes the increase in the current enhancement percentage (η%) where η%=2±0.07%, 15.8±0.93% and 21.6±1.04% for 1 h at −1.10, −1.20 and −1.30 V respectively, with the presence of PPMF. The nucleation and growth of the electrodeposition process were investigated, and it was concluded that the nucleation process was progressive at different applied potentials in the presence and absence of PPMF, from DMSO solvent. From the AFM results, the roughness factor of the alloy surface electrodeposited with PPMF was reduced compared to the alloy surface electrodeposited without PPMF for both deposition potentials. The electrodeposition of less noble metal (i.e., Fe) decreased and the more noble metals (i.e., Co and Ni) increased when done in the presence of PPMF. It was found that the layers with

larger content of noble metals showed more resistance towards corrosion than the layers with lower content of noble metals.

REFERENCES

[1] Brenner A. Electrodeposition of Alloys, vol. 2. New York: Academic Press; 1963.

[2] Verberne Wim MJC. Zinc–cobalt alloy electrodeposition. Trans Inst Met Fini 1986;64(1):30–2.

[3] Ohtsuka T, Komori A. Study of initial layer formation of Zn–Ni alloy electrodeposition by in situ ellipsometry. Electrochim Acta 1998;43(21–22):3269–76.

[4] Akiyama T, Fukushima H. Recent study on the mechanism of the electrodeposition of iron-group metal alloys. ISIJ Int 1992;32(7):787–98.

[5] Pál E, Dékány I. Structural, optical and photoelectric properties of indium-doped zinc oxide nanoparticles prepared in dimethyl sulphoxide. Coll Sur A 2008;318:141–50.

[6] Heo P, Ichino R, Okido M. ZnTe electrodeposition from organic solvents. Electrochim Acta 2006;51:6325–30.

[7] Fu J, Gao D, Xu Y, Xue D. The influences of electrodeposited temperature on the morphology and magnetic properties of Fe/Fe-dimethylsulfoxide nanocables. Electrochim Acta 2008;53:5464–548.

[8] Dahms H, Caroll IM. The anomalous codeposition of iron–nickel alloys. J Electrochem Soc 1965;112(8):771–5.

[9] Marikar YMF, Vasu KI. Electrodeposition of the ternary iron–cobalt–nickel alloy from the fluoborate bath part I. Deposition, anode corrosion, mechanism. Electrodep Sur Treat 1974;2(4):281–94.

[10] Lodhi ZF, Mol JMC, Hamer WJ, Terryn HA, De Wit JHWA. Cathodic inhibition and anomalous electrodeposition of Zn–Co alloys. Electrochim Acta 2007;52(17):5444–52.

[11] Roventi G, Fratesi R, Della Guardia RA, Barucca G. Normal and anomalous codeposition of Zn alloys from chloride bath. J App Electrochem 2000;30(2):173–9.

[12] Takahashi S, Aramata A, Nakamura M, Hasebe K, Taniguchi M, Taguchi S, et al. Electrochemica and in situ STM studies of anomalous phosphate adsorption induced on Zn UPD at Au(1 1 1) in the presence of halide ions in aqueous phosphate solutions. Surf Sci 2002;512(1–2):37–47.

[13] Higashi K, Fukushima H, Urakawa T, Adaniya T, Matsudo K. Mechanism of the electrodeposition of zinc alloys containing a small amount of cobalt. J Electrochem Soc 1981;128(10):2081–5.

[14] Lodhi ZF, Tichelaar FD, Kwakernaak, Mol JMC, Terryn H, de Wit JHW. A combined composition and morphology study of

electrodeposited Zn–Co and Zn–Co–Fe alloy coatings. Surf Coat Technol 2008;202(12):2755–64.

[15] Fukushima H, Akiyama T, Higashi K, Kammel R, Karimkhani M. Electrodeposition behavior of binary zinc alloy with iron-group metals from sulfate baths. Metal 1990;44(8):754–9.

[16] Po-Yu Chen, I-Wen Sun. Electrodeposition of cobalt and zinc–cobalt alloys from a lewis acidic zinc chloride-l-ethyl-3-methylimidazolium chloride molten salt. Electrochim Acta 2001;46:1169–77.

[17] Nicol MJ, Philip HI. Underpotential deposition and its relation to the anomalous deposition of metals in alloys. J Electroanal Chem 1976;70(2):233–7.

[18] Swathirajan S. Electrodeposition of zinc + nickel alloy phases and electrochemical stripping studies of the anomalous codeposition of zinc. J Electroanal Chem 1987;221(1–2):211–28.

[19] Lodhi ZF, Mol JMC, Hovestad A, Terryn H, de Wit JHW. Electrodeposition of Zn–Co and Zn–Co–Fe alloys from acidic chloride electrolytes. Surf Coat Technol 2007;202(1):84–90.

[20] Ebadi M, Basirun WJ, Alias Y, Mahmoudian MR. Normal and anomalous codeposition of Ni–Co–Fe–Zn alloys from EMIC/EG in the presence of an external magnetic field. Metall Mater Trans A 2011;42A:2402–10.

[21] Ebadi M, Basirun WJ, Alias Y, Mahmoudian MR. Electrodeposition of quaternary alloys in the presence of magnetic field. Chem Cent J 2010;4:14.

[22] Koza J, Uhlemann M, Gebert A, Schultz L. The effect of magnetic fields on the electrodeposition of iron. J Sol Stat Electrochem 2008;12(2):181–92.

[23] Bund A, Koehler S, Kuehnlein HH, Plieth W. Magnetic field effects in electrochemical reactions. Electrochim Acta 2003;49:147–52.

[24] Tabakovic I, Riemer S, Vas'ko V, Spozhnikov V, Kief M. Effect of magnetic field on electrode reactions and properties of electrodeposited NiFe films. J Electrochem Soc 2003;150: C635–40.

[25] Aaboubi O, Chopart JP, Douglade J, Oliver A, Gabrielli C, Tribollet B. Magnetic field effects on mass transport. J Electrochem Soc 1990;137:1796–804.

[26] Soto AB, Arce EM, Palomar-Pardavé M, González I. Electrochemical nucleation of cobalt onto glassy carbon electrode from ammonium chloride solutions. Electrochim Acta 1996;41(16):2647–55.

[27] Lioubashevski O, Katz E, Willner I. Effects of magnetic field directed orthogonally to surfaces on electrochemical processes. J Phys Chem C 2007;111:6024–32.

[28] Lioubashevski O, Katz E, Willner I. Magnetic field effects on electrochemical processes: a theoretical hydrodynamic model. J Phys Chem C 2004;108:5778–84.

[29] Ebadi M, Basirun WJ, Alias Y. Influence of magnetic field on the electrodeposition of Ni–Co alloy. J Chem Sci 2009;112(2):279–85.

[30] Ebadi M, Basirun WJ, Alias Y. Influence of magnetic field on the mass electrodeposition and investigation of corrosion rate on Ni and Ni–Co alloy. Asian J Chem 2009;21(8):6343–53.

[31] Ebadi M, Basirun WJ, Alias Y. Influence of permanent perpendicular magnetic field on the electrodeposition of nickel. Asian J Chem 2009;21(9):7354–62.

[32] Basirun WJ, Pletcher D, Reintjes AS. Studies of platinum electroplating baths part IV: deposits on copper from Q bath. J App Electrochem 1996;26:873–80.

[33] Basirun WJ, Pletcher D. Studies of platinum electroplating baths part VI: influence of some experimental parameters on deposit quality. J App Electrochem 1997;28:167–72.

[34] Ispas A, Matsushima H, Bund A. On the p-doping of PEDOT layers in various ionic liquids studied by EQCM and acoustic impedance. Electrochim Acta 2009;54(20):4668–75.

[35] Zielinski M, Miekos E. Influence of constant magnetic field on the electrodeposition of Co–Mo–W alloys). J Appl Eelectrochem 2008;38(12):1771–8.

[36] Fahidy TZ. Characteristics of surfaces produced via magnetoelectrolytic deposition. Prog Surf Sci 2001;68:155–88.

[37] Mansfeld F, Kendig MW, Tsai S. Evaluation of corrosion behavior of coated metals with AC impedance measurements. Corrosion 1982;38:478–85.

[38] Scully JR, Hensley ST. Lifetime prediction for organic coatings on steel and a magnesium alloy using electrochemical impedance methods. Corrosion 1994;50(9):705–16.